Journal of Marine Science and Application (2026) 25: 46-62
https://doi.org/10.1007/s11804-025-00685-6

RESEARCH ARTICLE

Numerical Analysis and Geometric Assessment of Air Layer Distribution in a Ventilated Planing Hull in Calm Water

Massimiliano Chillemi[1], Filippo Cucinotta[1] and Felice Sfravara[1]

Received: 30 October 2024 / Accepted: 16 January 2025

Abstract

The issue of resistance reduction through hull ventilation is of particular interest in contemporary research. This paper presents multiphase computational fluid dynamics (CFD) simulations with 2-DOF motion of a planing hull. The original hull was modified by introducing a step to allow air ventilation. Following an assessment of the hull performance, a simulation campaign in calm water was conducted to characterize the hull at various forward speeds and air insufflation rates for a defined single step geometry. Geometric analysis of the air layer thickness beneath the hull for each simulated condition was performed using a novel method for visualizing local air thickness. Additionally, two new parameters were introduced to understand the influence of spray rails on the air volume beneath the hull and to indicate the primary direction of ventilated air escape. A validation campaign and an assessment of uncertainty of the simulation has been conducted. The features offered by the CFD methodology include the evaluation of the air layer thickness as a function of hull velocity and injection flow rate and the air volume distribution beneath the hull. The air injection velocity can be adjusted across various operating conditions, thereby preventing performance or efficiency loss during navigation. Based on these findings, the study highlights the benefits of air insufflation in reducing hull resistance for high-speed planing vessels. This work lays a robust foundation for future research and new promising topics, as the exploration of air insufflation continues to be a topic of contemporary interest within naval architecture and hydrodynamics.

Keywords Computational fluid dynamics; Air cavity ships; Planing hull; Hydrodynamics; Maritime sustainability

1 Introduction

1.1 Planing hulls

A planing hull is a specific type of hull design that distinguishes itself by its ability to plan across the water surface rather than cutting through it like a displacement hull. These hulls are commonly found in high-speed boats such as powerboats and water ski boats. The key characteristic of a planing hull is its relatively flat and narrow shape. This design allows the hull to rise and glide above the water at high speeds, thereby reducing hull resistance and improving overall efficiency. Additionally, planing hulls tend to have a shallow draft, meaning they do not sit too deeply in the water, which further minimizes hull resistance.

Achieving planing in these hulls relies on multiple factors, including the hull shape, engine power, and the surface area in contact with the water. The hydrodynamic behaviour can also be influenced by the presence of devices such as trim tabs. Planing hulls are particularly popular in recreational boating due to their ability to provide a smooth and comfortable ride even at high speeds. However, they can be more challenging to handle at lower speeds and may exhibit less stability compared to other hull types in rough water conditions. This is because at lower speeds, a planing hull does not generate enough lift to rise out of the water. Instead, it behaves more like a displacement hull, pushing through the water rather than riding on top of it and the hydrodynamic forces acting on the hull at these speeds are not optimized for stability and control, leading to less predictable handling. The stability issues at lower speeds are also caused by the displaced volume and by the

Article Highlights

- Air cavity ships (ACS) reduce hydrodynamic resistance, fuel consumption, and emissions injecting air under the hull.
- These hulls benefit from air cavity lubrication, which minimizes friction and enhances energy efficiency, though challenges remain in understanding air distribution dynamics.
- A novel tridimensional visualization method was introduced in this work to evaluate local air cushion thickness, addressing a key research gap in ACS technology.
- The study proposed two new parameters, Air Direction Ratio and Spray Rails Airflow Fraction, to improve hull ventilation assessment.

✉ Massimiliano Chillemi
massimiliano.chillemi@unime.it

[1] Department of Engineering, University of Messina, Contrada Di Dio s. n. c. 98166, Messina, Italy

centre of pressure movement during motion. Planing hulls have a shape that displaces less water compared to displacement hulls when they are moving slowly. This reduced displacement means less buoyancy and less ability to counteract the effects of waves and other external forces, contributing to instability. Regarding the centre of pressure, this can shift significantly with any subtle vertical movement of the hull. At high speeds, the centre of pressure is relatively stable because the hull is skimming over the surface. At lower speeds, the hull is more submerged, and even small changes in vertical position can cause large shifts in the centre of pressure, leading to unpredictable changes in balance and handling. The performance of a planing hull is influenced by various factors that can be improved to enhance its capabilities. For instance, optimizing the hull shape plays a crucial role in reducing hull resistance and increasing stability. Ensuring the engine power matches the boat's size and weight is vital to generating the necessary lift without compromising stability. Managing the surface area in contact with the water helps strike a balance between lift and hull resistance.

A well-designed hull can significantly improve the seakeeping behaviour of a planing vessel. This can be achieved by carefully selecting fundamental design factors such as the deadrise angle, length-to-beam ratio or the angle and position of spray rails. Additionally, proper weight distribution throughout the ship contributes to improved stability and handling. By addressing these factors, it is possible to enhance the performance of a planing hull, enabling higher speeds, improved manoeuvrability, and increased stability.

1.2 Frictional resistance reduction with air cavities

The initial idea for air cavities under a flat bottom planing hull dates to 1882 with a first US patent being deposited that year. Other patents were later registered from 1908 to 1912 as written by Latorre (1997). In 1968 theoretical and experimental investigations were conducted on the reduction of ships frictional resistance by blowing air under their bottom by Basin et al. (1968). This concept was later applied to ships through full-scale trials of a boat with an air cavity (Butuzov et al., 1988). Several studies have investigated the principal characteristics of air cavities under various conditions, employing experimental and numerical tests in different forms. A review about hull resistance reduction techniques was made by Ahmadzadehtalatapeh and Mousavi (2016).

Matveev (2003) identified the parameters and the devices influencing the air cavity using numerical studies for a simplified configuration. Apart from Froude number and cavitation number, one of the parameters is the wedge angle at the rear of the hull that influences the formation and stability of the cavity, with an optimal angle helping to minimize air leakage. The influence of the propulsor is also crucial: correct positioning and characteristics of the propulsor are necessary to maintain cavity stability. If the propulsion units are positioned in the vicinity of the cavity end, they can a negative impact. Devices like interceptors and trim tabs can optimize pressure distribution and enhance cavity stability if they are placed at the transom.

The influence of hydrofoils under the cavity depends on their positioning. Experimental tests on displacement hulls with air ventilated cavities were conducted by Butterworth et al. (2015) and Amromin (2016). Regarding planing hulls, fewer experimental and numerical tests have been conducted. Matveev (2015) proposed a numerical method for predicting hull resistance reduction validated with experimental data, and Matveev (2020) applied a potential-flow theory for modelling the air cavities under solid walls in water flow with fluctuating pressure.

Gokcay et al. (2004) conducted experimental work analysing total resistance, trim, sinkage, and wave patterns for high-speed crafts with artificial air cavities. This study proved that, after the air injection, the trim angle increased in the specific studied regime. This finding was evident in the research, which compared different hulls: one without air injection (denoted as AC0) and others with varying rates of air injection (denoted as AC1 and AC2). Both AC1 and AC2 displayed higher trim angles than the conventional prismatic planing hull form (denoted as HC). These experimental data are not only important for better understanding the artificial air cavity phenomenon but also for validating numerical methods such as unsteady Reynolds-averaged Navier Stokes equation (URANSe) methods for this kind of problem. In recent years, numerical methods have been widely used both for structural optimization (Barberi et al., 2022; Cucinotta et al., 2021b, 2020; Deng and Suresh, 2017; Plocher and Panesar, 2019; Yan, 2021) and for fluid-dynamics purposes (CFD).

CFD methods play a crucial role in the design and optimization of ships at all stages, offering capabilities that extend beyond single-goal optimization to holistic approaches.

For instance, traditional applications of CFD include single-goal optimizations such as minimizing ship resistance, enhancing seakeeping behaviour, or designing optimized propulsion systems.

CFD is particularly useful in modelling fluid flow around planing hulls, specifically those with air injection. This advanced application allows for capturing fully non-linear fluid motion around the vessel, monitoring vorticity generation, and observing the creation of air-water mixtures, which are critical features for the performance and efficiency of planing hulls with air injection.

These simulations provide significant insights, enabling more precise and effective design modifications to improve overall vessel performance. Different studies were performed on trimaran hulls (Nazemian and Ghadimi, 2021a, 2021b; Nazemian and Ghadimi, 2022a), underwater vehi-

cles (Hou et al. (2022) and Chen et al. (2023), which combines CFD with genetic algorithms), to perform CAD-based optimization (Nazemian and Ghadimi, 2022b) and finally on planing hulls (Diez et al., 2022; Ghadimi et al., 2023; Sulman et al., 2024). Other similar studies are about hydrodynamic hull shape optimization (Gao et al., 2016) and aerodynamic shape optimization using machine learning techniques (Yan et al., 2019). In the case of air cavity ships (ACS), the problem of multiphase flow with interaction between different scales is a significant challenge (Cucinotta et al., 2017a; Cucinotta et al., 2017b; Pearce et al., 2015).

Tavakoli et al. (2024) carefully review studies on planing hulls and discusses the research challenges. One of the main research challenge lies on developing mathematical and numerical models that can capture with high fidelity the complex interaction between hulls and marine environment. In particular, there is an important research gap regarding models that can describe stepped planing hulls.

The behaviour of planing hulls is also influenced by the effect of longitudinal rails: Cucinotta et al. (2021a) made a comparison between towing tank tests and CFD analyses carried out on a single-step planing hull with forced ventilation on the bottom. The air-water interface effects for ACS have been investigated by the simulation of pre-planing behaviour modelling with the aim of capturing the interface effects, comparing resistance, dynamic trim, and wetted surface area in Nimmagadda et al. (2020). The implantation of air lubrication can lead to fuel, emissions and costs savings: this could be seen with a Life Cycle Assessment which has already been made for different naval applications (Busetto et al., 2022; Cucinotta et al., 2021c; Di Bernardo et al., 2024; Mio et al., 2022). Currently, only a few studies have been conducted to understand the distribution of air under the hull during the injection process. Specifically, in the field of yacht design, there is limited knowledge about this phenomenon. The complexity of the air injection process in this context is further compounded by the varying positions of the hull at different speeds, such as pre-planing and planing.

The main objective of this paper is to reduce the knowledge gap regarding the phenomena of air injection under the hull, focusing on the distribution of air thickness and the bottom view of the ventilated area. This will be achieved through a methodology suitable for use in the early stages of project development.

Understanding the spatial distribution of the air layer during the injection process is crucial for assessing its impact on hull architecture. These impacts concern the effective reduction of hull resistance and the effects on the trim and sinkage of the hull. It is fundamental to evaluate all these impacts in the early stage of the design or in the case of retrofitting processes.

This paper introduces a CFD methodology for assessing the reduction of hull resistance through air injection compared to the original hull. Additionally, it evaluates characteristics that cannot be assessed with generic towing tank tests. The main features provided by the CFD methodology include the assessment of the air layer thickness as a function of hull velocity and injection speed, the stability of the air layer, and the volume and distribution of air under the hull.

The objective of the study is to enhance understanding of air cavity phenomena through a geometric analysis of the air ventilated under the hull in various conditions. The studied hull is a 13-meter Fast Coast Guard Boat. The CFD simulations are performed using Simcenter STAR-CCM+, while the geometric analyses are conducted with MeshLab (Cignoni et al., 2008) and Matlab.

The forthcoming of the paper is as follows:

• Section Materials and Methods explains the main characteristic of the hull, the workflow and the range of velocities simulated, the setup of the CFD simulation in terms of numerical methods and type of mesh used. In addition, in this section is explained the user function used for the post-processing of the results in terms of volume of air under the hull.

• Results section highlights the main effects of the air injection with respect to the original hull, a general assessment of the volume of the air under the hull and the distribution of the air.

• Conclusion chapter provide a resume of the main topics of the paper with particular attention on future developments, impacts of these results on naval architecture.

• Appendix A provides the mesh sensitivity analysis conducted following the procedure suggested by ITTC.

• Appendix B provides a verification of the CFD setup used in the paper exploiting experimental tests conducted previously and published in (Cucinotta et al., 2021a, 2019, 2018a, 2018b, 2017a, 2017b).

• In the section Nomenclature all the symbols used inside the paper are explained and defined.

2 Materials and methods

2.1 Hull geometry

The hull under study is a typical planing hull. A planing hull is a type of boat designed to lift and skim on top of the water at high speeds, rather than displacing water. The main characteristics of a planing hulls are a flat or V-shaped bottom that allows them to rise and glide over the water surface. An important dimension for this kind of feature is the angle of deadrise.

Another characteristic of these hulls is the hard chine, it is a sharp edge along the bottom sides of the hull. Usually, these types of hulls are resigned with an emphasis on reduc-

ing water resistance and maximizing lift. The fundamental geometric characteristics of the planing hull under investigation are reported in Table 1. The original hull does not include a step that was added to be able to inject the air. All the main dimensions of the original hull have been kept the same. The hull has a constant deadrise angle equal to 20° along the vessel length, this value is a good compromise between comfort and velocity performance. The value of the beam at the transom is 3.8 m and the beam change along the vessel reaching the maximum value of 3.93 m. The hull geometry is represented in Figure 1, in particular in Figure 1(c) the dimensions relative to the deadrise angle and the height of the step are showed.

Table 1 Main dimensions of the hull

L_{OA} (m)	14.50
L_H (m)	13
BPT (m)	3.80
BPX (m)	3.93
DPT (m)	2.23
DFT (m)	0.76
β (°)	20
Δ (t)	15
L_{CG} (m)	4.20
V_{CG} (m)	1
N_{ST}	1
L_{ST} (m)	4.40
$B_{IN} \times H_{IN}$ (m×m)	1.72 × 0.055

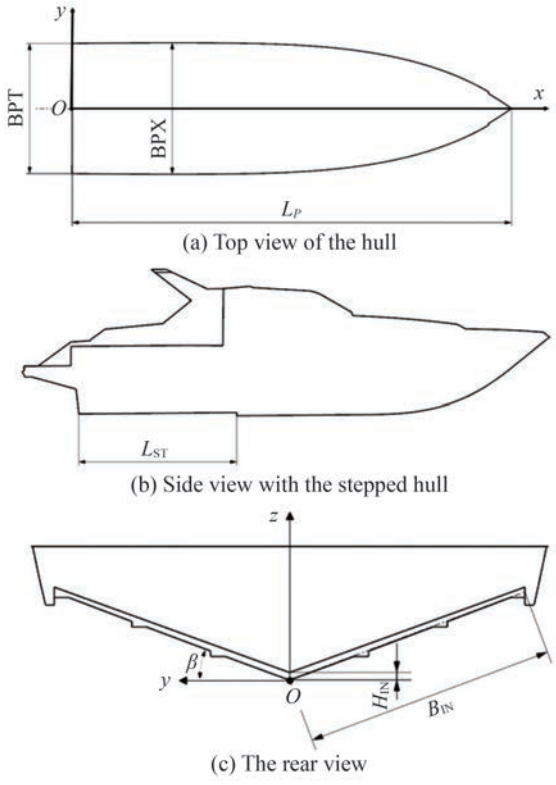

Figure 1 Geometry of the hull

2.2 Study workflow

The implemented CFD model is useful for solving the velocity and pressure fields around the hull and its motion in terms of trim and sinkage.

The fluid is considered viscous and incompressible, the interaction between the water and the air is considered thanks to a simulation multiphase. Simulations were conducted using Simcenter STAR-CCM+.

A speed range was defined to properly characterize the hull, starting from a non-planing condition and gradually reaching the intended planing condition.

Initially, a comparison was made between the performance of the original (baseline) hull and the hull with the step in the absence of air cavities.

After confirming that the total resistance and trim remained largely unchanged, especially within the operating range, a simulation campaign was initiated to test the hull with the step at five different speeds.

The simulation with air injection is also categorized by the Flow Rate Coefficient (CQ) as suggested by Cucinotta et al. (2017a).

CQ is defined as the ratio between the injected air velocity and the hull velocity. Each simulation with air injection has an ID: this is obtained considering the hull velocity V_H in knots and the adopted CQ value (ID: V_H [kn]_CQ).

The campaign of simulation is reported in Table 2.

In the simulation with air injection, three different air speeds were tested for each hull speed.

Once the simulations were completed, a Java macro was developed to be executed within the Simcenter STAR-CCM+ environment to extract the volumes of air cavities beneath the hull for each tested condition.

The volumes are processed in MeshLab to obtain the main geometrical characteristics and the data from the CFD simulation and the volume analysis is then processed in Matlab.

2.3 CFD Setup

The CFD setup proposed in the paper is used to study the air layer distribution in terms local thickness, the hull resistance reduction due to air injection and all the physical quantities that describe the hull behaviour in the water such as trim and sinkage. The unsteady Reynolds averaged Navier Stokes (URANS) equations are solved using an implicit solver with an adaptive time step calculated to satisfy the condition of the courant number being equal to or less than 1. To solve the pressure and velocity fields, a Segregated Flow approach is employed, with the momentum and continuity equations connected through a predic-

Table 2 Tests on baseline hull and stepped hull

Configuration	Simulation ID	V_H (kn)	V_H (m/s)	CQ	V_A (m/s)	Fn
Baseline design	12_BL	12	6.17	–	–	0.55
	18_BL	18	9.26	–	–	0.82
	24_BL	24	12.35	–	–	1.09
	30_BL	30	15.43	–	–	1.37
	36_BL	36	18.52	–	–	1.64
Stepped hull, no air injection	12_0	12	6.17	–	–	0.55
	18_0	18	9.26	–	–	0.82
	24_0	24	12.35	–	–	1.09
	30_0	30	15.43	–	–	1.37
	36_0	36	18.52	–	–	1.64
Stepped hull with air injection	12_1	12	6.17	1	6.17	0.55
	12_2	12	6.17	2	12.34	0.55
	12_3	12	6.17	3	18.51	0.55
	18_1	18	9.26	1	9.26	0.82
	18_2	18	9.26	2	18.52	0.82
	18_3	18	9.26	3	27.78	0.82
	24_1	24	12.35	1	12.35	1.09
	24_2	24	12.35	2	24.70	1.09
	24_3	24	12.35	3	37.05	1.09
	30_1	30	15.43	1	15.43	1.37
	30_2	30	15.43	2	30.86	1.37
	30_3	30	15.43	3	46.29	1.37
	36_1	36	18.52	1	18.52	1.64
	36_2	36	18.52	2	37.04	1.64
	36_3	36	18.52	3	55.56	1.64

tor-corrector method. For all simulations, the turbulence model employed is the realizable $k-\varepsilon$ two-layer model. The algebraic system of equations is solved using an algebraic multigrid method. The hybrid method Gauss-least square (Gauss-LSQ) is utilized to solve gradients during the discretization process, combining aspects of the Gauss and Least Square methods. A time-marching approach is adopted for each simulation to capture unsteady phenomena, employing first-order temporal discretization. In addition to the Navier-Stokes equations, an additional transport equation is solved for the volume fraction of the two immiscible fluids. The volume of fluid (VOF) method is considered for this purpose. The high-resolution interface capturing (HRIC) scheme is employed for convection in the VOF method, ensuring a sharp interface between the immiscible fluids. During the simulations, the planing hull is allowed to pitch and heave. To accurately capture the strong interaction between air and water, multiphase interaction is incorporated with a surface tension of 0.072 N/m imposed between the two fluids. An important concern in these studies is numerical ventilation. To recover and prevent ship hull ventilation, a User-Defined Slip Velocity approach was implemented within the VOF framework. Numerical ventilation, which refers to the undesirable mixing of phases, is a common issue in marine simulations. This Slip Velocity approach, integrated within the VOF framework, functions by algebraically computing distinct velocities for the two phases when they coexist, thereby enabling the separation of air from water and restoring the interface. A distinguishing feature of the VOF Slip Velocity model, which sets it apart from other techniques aimed at reducing numerical ventilation, is its physical basis. This aspect allows for its utilization in scenarios where the presence of air is expected in the solution, such as in stepped hulls. The method is presented in detail in Wheeler et al. (2021). The Dynamic Fluid Body Interaction solver is activated, enabling the evaluation of hydrodynamic forces within each time step and solving the rigid body equations (Newton second law) to determine hull sinkage and trim. A minimum of five inner iterations are performed to determine the new position of the ship for each time step. The mesh motion resulting from the hull movement is managed using the

overset technique, which is more advantageous for high-speed ships than the morphing methodology. This technique ensures minimal degradation of cell elements, particularly at high trim angles, while maintaining high accuracy near all boundaries. A linear interpolation scheme is employed to link results between the background region and the overset region. Table 3 provides a summary of the setup for the numerical simulation.

Table 3 Physics models of the CFD simulation

Discretization method	Finite volume method
Solver	Implicit unsteady
Approach	Segregated flow
Continuity and momentum equation coupling	SIMPLE Algorithm
Convection term	2nd order
Turbulence model	Realizable $k-\varepsilon$ two-layer
Temporal discretization	1st order
Iteration for time step	5
Maximum courant number per time-step	1
Gradient discretization	Hybrid Gauss-LSQ
Algebraic system of equations solver	Algebraic multigrid solver (AGM)
Interface	VOF
Convection scheme for VoF	HRIC
Ship hull motion	Dynamic fluid body interaction (DFBI)
Inner iterations for ship motion DFBI	10
Mesh motion	Overset mesh
Interpolation for overset	Linear

The background volume is a block with a length of 100 m, a width of 40 m and a height of 80 m.

The boundary conditions are illustrated in Figure 2 (background region); the figure shows also the level of the water and the reference frame used during the simulation. The -*Y* surface that closes the block (not represented) has a Symmetry boundary condition.

Figure 3 shows the boundary conditions applied to overset region, and in particular the velocity inlet boundary condition applied on the step surface to inject air. The VOF wave model has been used to define the volume fraction, the magnitude and the direction of the velocity on the Velocity Inlet boundaries. Being the simulations in calm water, the selected VOF wave model is the flat wave. The flat wave is the boundary condition imposed inside the numerical setup in order to simulate a state of calm sea without waves. With this condition it is possible to fill with the water the background volume and the overset volume and to apply a constant velocity to the flow.

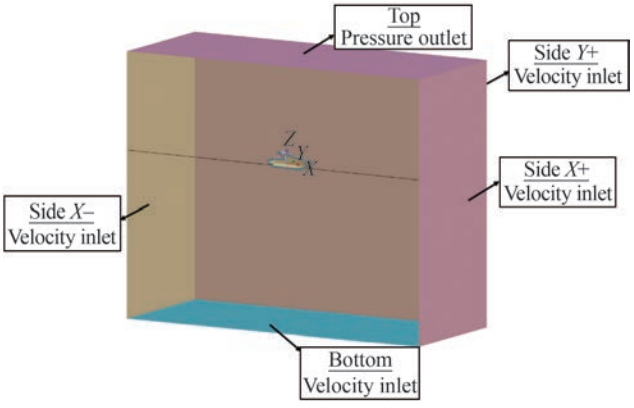

Figure 2 Boundary conditions of the background volume

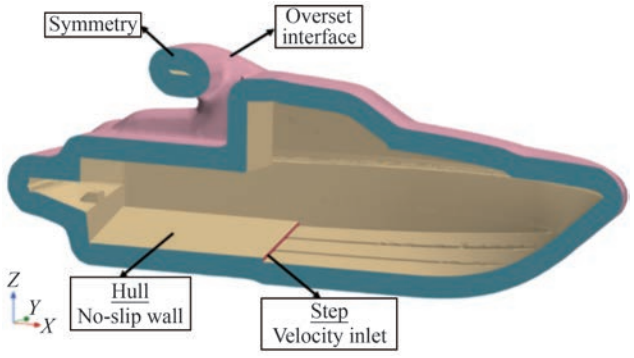

Figure 3 Boundary conditions of the overset volume

The simulation results are relative to a navigation condition of the boat in calm water without waves.

The overset volume has been obtained offsetting the surface of the ship in the outer direction. The step is defined as a Velocity Inlet of only air and the velocity magnitude depends on the CQ value.

The mesh is a trimmed cell mesh, with the base size being 3% of BPX for the overset region. For the hull, the minimum surface cell size is 1.5% of BPX, while the mesh of the background region goes up to 63% of BPX. The minimum size for the Background goes down to 15% to refine the Interface and the volume around the overset. The overset mesh is displayed in Figure 4.

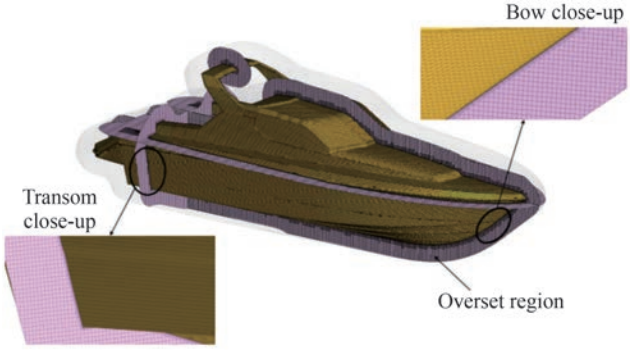

Figure 4 Overset mesh

The CFD setup proposed in the paper has been validated in the Appendix A and an uncertainty analysis has been reported in Appendix B.

2.4 Macro for volume and mass flow rate extraction

The Java macro performs several operations to extract the air volume under the hull and the values of the mass flow rates.

Firstly, it isolates, from the entire fluid region, only the portion with an air volume fraction between 0.5 and 1. Once this portion of the volume is isolated, the macro performs a Boolean intersection between the obtained volume and a known-sized block (air control volume) positioned beneath the hull, between the step and the transom. The Boolean intersection is then exported in STL format and the air volume is therefore obtained.

To extract the values of mass flow rates, three surfaces are defined as in Figure 5. The macro then creates three reports of air mass flow rate (one for each surface) and the results are written to an output file.

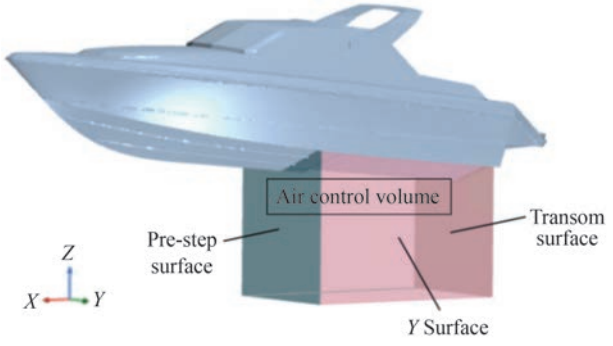

Figure 5 Surfaces of the control volume

2.5 Volume analysis in meshlab

The Metro tool (Cignoni et al., 1998) utilizes Hausdorff's method to calculate distances between points and surfaces. The distance between a point p and a surface S, denoted as $e(p, S)$, is defined as the minimum Euclidean distance between p and any point p' on S.

$$e(p, S) = \min\left(d(p, p')\right), p' \epsilon S \tag{1}$$

For each condition, the distance was calculated by considering two surfaces extracted from the STL file exported from Star-CCM+: the upper face and the lower face of the air layer. To determine the distance between two surfaces, S_1 and S_2, the tool calculates $E(S_1, S_2)$ as the maximum distance between any point in S_1 and surface S_2. Afterwards, the tool assigns a coefficient to each distance, ranging from 0 to 1, and maps it to an RGB colour scale using a piecewise linear transfer function. The colour gradient transitions from red to blue as the distance between the air layer on the hull and the bottom part of the air volume increases.

3 Results

3.1 Definition of the step's position

The baseline hull, as mentioned before, is without step. In order to inject the air, a step must be positioned under the hull. The primary goal of the step is not to produce natural ventilation along the sides, as is commonly seen in the design of planing hulls. Instead, the design and positioning of the step at this stage are not guided by this principle. The main objective in this phase is to have the step completely submerged during all the navigation condition of the boat.

This condition guarantees that the injected flow rate is not dispersed directly in air.

In order to find the right position of the step, a first simulation was conducted to establish its position, which has to serve as air inlet. The step must be always submerged to maximize the effect of the air injection. To determine the position of the step, a simulation of the baseline hull at Fn = 1.64 (corresponding to its maximum velocity by design) was made. This also represents the operating condition with the lowest wetted surface.

The results (Figure 6) show that the hull, in its equilibrium condition, is submerged for 4.4 m starting from the transom (L_{ST} = 4.4 m). The step was then positioned at this distance because it is crucial for the air to be injected into a consistently submerged area to fully appreciate the effect of air injection.

In the same picture it is possible to appreciate also the

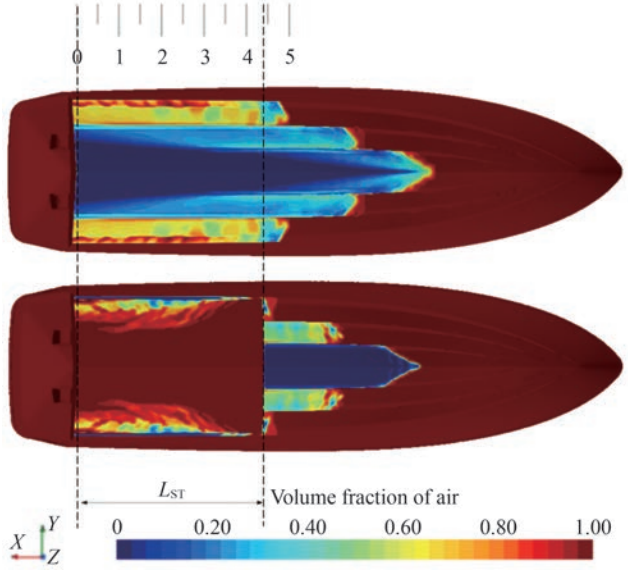

Figure 6 Comparison between baseline and stepped hull at Fn = 1.64 with CQ3

great work conducted by the VOF Slip Velocity method in conjunction with HRIC algorithm. Along the centreline of the hull, no air is trapped by the numerical ventilation.

3.2 Comparison between baseline and stepped hull

The baseline hull and the stepped hull without air injection were tested at the velocities listed in Table 2. The simulation results are presented in Table 4.

The hull resistance has been reported after normalizing it with the displacement Δ.

The total hull resistance shows a slight increase with the stepped design at Froude numbers (*Fn*) below 1 and decreases for *Fn* values exceeding 1. At *Fn* = 1.64, the hull resistance of the stepped design is the 85% of the baseline one. It can be also observed that the trim angle of the boat remains essentially unchanged in the stepped version, meanwhile the wetted surface area is lower in the stepped version for all tested velocities. From these results, it can be said that the step introduced in the hull did not worsen the performance, given that the trim angle is almost unchanged and that the hull resistance is slightly increased in the non-planing region, meanwhile it's lower in the planing region (which represents the operating condition, so the condition of interest). Therefore, the stepped hull can be studied with air injection. After confirming that the modification made to the baseline hull did not negatively alter the behaviour of the ship, simulations were conducted with air injection. The simulations were performed, and the results related to the main hydrodynamic quantities are presented in Table 5, including the normalized wet area $S_{w,n}$.

$$S_{w,n} = \frac{S_w}{S_w + S_v} \tag{2}$$

S_w is the wet area and S_v is the ventilated area: both are extracted from the CFD simulations for every *Fn* and every CQ.

The complement to 1 of $S_{w,n}$ represents the normalized ventilated area $S_{v,n}$.

The results collected in Table 4 and Table 5 have been represented in graphs from Figure 7 to Figure 9. For each graph, the examined quantity has been plotted against the Froude number of the hull, with each curve parameterized based on the value of CQ. In Figure 7, the trend of hull resistance for different velocities is shown. Below *Fn* = 1.09, as the air ventilation velocity increases, there is an increase in the total resistance since the reduction of the wetted surface area is not compensating for the increase in pressure resistance caused by the higher trim angle. Above *Fn* = 1.09, this trend reverses, with resistance decreasing as the value of CQ increases.

From Figure 8, it is evident that at higher air velocities, the trim angle values increase up to *Fn* = 1.09 (therefore still in semi-planing conditions). However, above *Fn* = 1.09, as the air velocity increases, the trim angle decreases.

Considering Figure 9, it can be observed that the wetted surface area decreases as the Froude number increases. For *Fn* = 0.55, there is not a clear change in wetted area as the CQ increases. The hull dries evidently with the increasing of CQ for *Fn* = 0.82 and *Fn* = 1.09 and then the effect of CQ becomes again less influent for higher Froude numbers.

Table 4 Results from simulations on baseline and stepped hull without air injection

Fn	Hull resistance normalized with displacement			Trim (°)			Normalized wet area		
	CQ1	CQ2	CQ3	CQ1	CQ2	CQ3	CQ1	CQ2	CQ3
0.55	0.143	0.142	0.140	5.5	5.5	5.5	0.830	0.808	0.828
0.82	0.166	0.168	0.174	7.1	7.4	7.9	0.641	0.579	0.559
1.09	0.154	0.157	0.157	6.8	7.3	7.5	0.413	0.367	0.363
1.37	0.128	0.124	0.120	5.2	5.1	4.9	0.342	0.342	0.334
1.64	0.109	0.105	0.104	3.8	3.7	3.7	0.265	0.261	0.257

Table 5 Results from simulations on stepped hull with air injection

Fn	Hull resistance normalized with displacement			Trim (°)			Normalized wet area		
	CQ1	CQ2	CQ3	CQ1	CQ2	CQ3	CQ1	CQ2	CQ3
0.55	0.143	0.142	0.140	5.5	5.5	5.5	0.830	0.808	0.828
0.82	0.166	0.168	0.174	7.1	7.4	7.9	0.641	0.579	0.559
1.09	0.154	0.157	0.157	6.8	7.3	7.5	0.413	0.367	0.363
1.37	0.128	0.124	0.120	5.2	5.1	4.9	0.342	0.342	0.334
1.64	0.109	0.105	0.104	3.8	3.7	3.7	0.265	0.261	0.257

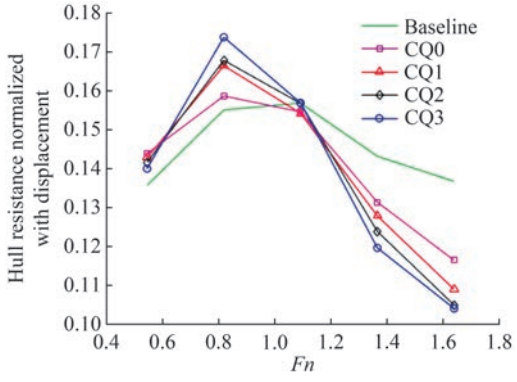

Figure 7 Hull resistance at different hull and air velocities

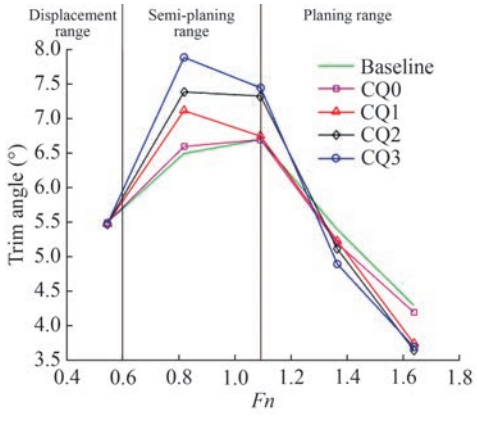

Figure 8 Trim angle at different hull and air velocities

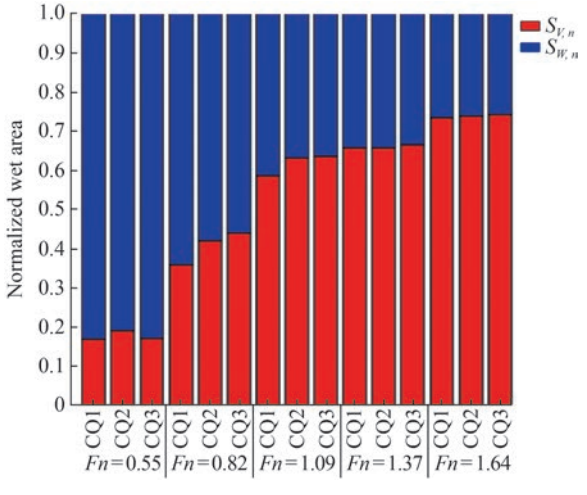

Figure 9 Bar plot of normalized wet and ventilated area

For greater clarity, using the data in Table 4 and Table 5, the trend of the relative change in hull resistance with respect to the baseline design has been calculated and it's reported in Figure 10. The plot once again highlights how the greatest benefits are obtained under planing conditions, with the hull resistance going down to the 76% of the baseline value at 36 kn for CQ3. To further highlight the contributions of air injection on resistance, the total resistance was divided into two components: frictional resistance, which is mainly influenced by air injection, and pressure resistance, which accounts for other resistance phenomena, including wave formation. It was observed that air injection consistently reduces frictional resistance, but at low Froude numbers, it leads to an increase in pressure resistance due to the wave patterns generated.

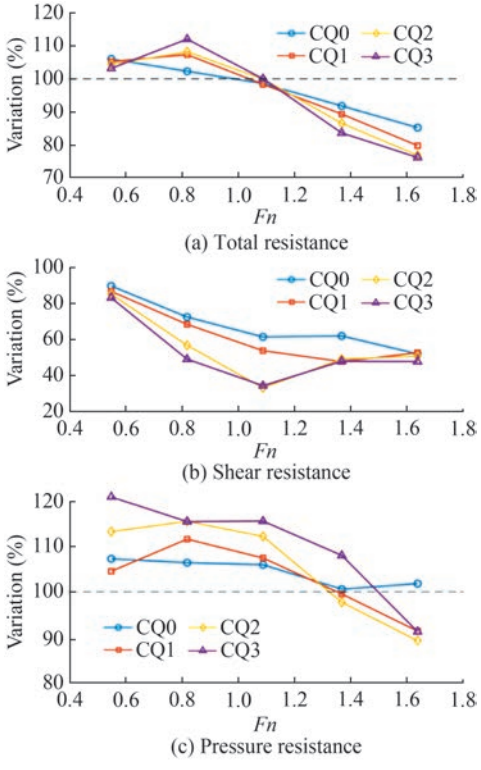

Figure 10 Percentage of hull resistance change referred to the baseline design

From the analysis of the results, it emerges that the *Fn* = 1.09 can be considered as a critical speed, above which the behaviour of the hull changes between non-planing and planing conditions. Above *Fn* = 1.09 and under *Fn* = 1.37 (operating conditions of the hull), with the aim of reducing the total resistance to advancement, it is not advantageous to consider values of CQ greater than 2 since an increase in the air velocity does not correspond to an important hull resistance reduction.

Additionally, a comparison at the maximum Froude number was made between the original hull and the CQ3 hull, with the wave profile plotted at four different distances behind the hull.

It was found that air injection does not significantly alter either the peaks or the frequencies of the wave. Slight increases in peak values were observed for CQ3, which justifies the absence of significant benefits in pressure resistance reduction under these conditions.

Results related to sinkage for each Froude number and each CQ were also extracted from the CFD simulations. The sinkage has been normalized dividing it by the draft DFT: the normalized values are reported in Table 6.

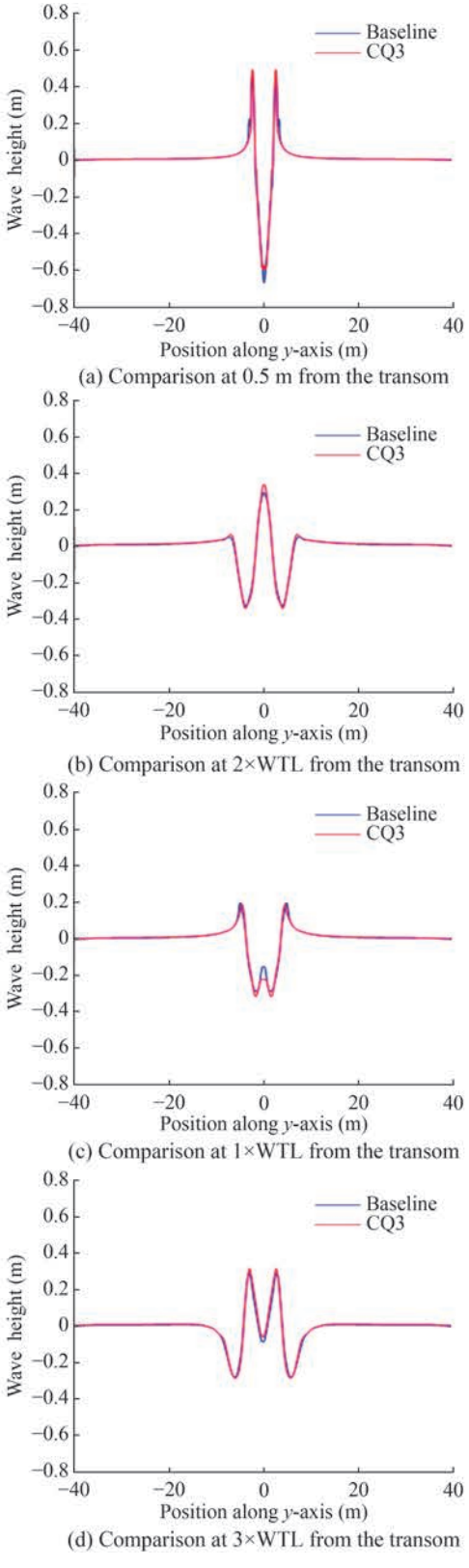

Figure 11 wave profiles comparison at $Fn = 1.64$

3.3 Geometric assessment of the air layer

This paragraph presents the results obtained from the analysis conducted on MeshLab on the volumes of air. Figure 12, Figure 13 and Figure 14 show contour plots that display, for each CQ condition and varying hull velocity, a map depicting in the lower half of the hull the local normalized thickness of the air layer trapped beneath the hull. Unlike the conventional area-based representation system that allows to see just where the wet and ventilated areas are, this new system permits the visualization of the local thicknesses of the air layer. This is of great interest as it reveals the effects associated with the presence of spray rails and the phenomenon of lateral air flow escape effect. To improve the visualization of the phenomenon, in the upper half of the hull a Volume Fraction of Water contour has been represented.

Table 6 Normalized sinkage

Fn	Sinkage normalized with draft				
	BL	CQ0	CQ1	CQ2	CQ3
0.55	−0.036	−0.050	−0.043	−0.050	−0.042
0.82	0.223	0.224	0.237	0.250	0.276
1.09	0.488	0.487	0.513	0.566	0.592
1.37	0.619	0.618	0.671	0.697	0.724
1.64	0.712	0.711	0.724	0.737	0.750

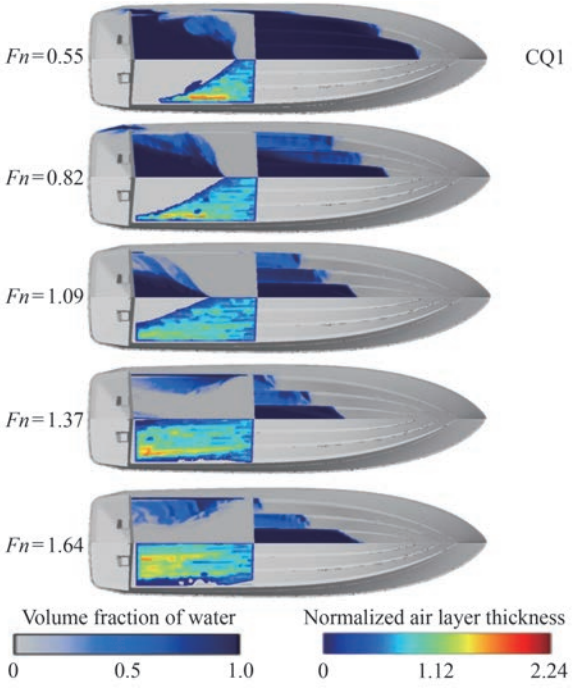

Figure 12 Air layer thickness and volume fraction of water contour plot for CQ1

To normalize the air layer thickness, a mean boundary layer height δ has been calculated. This calculation is based on the Reynolds number: a mean value of the tested velocities has been considered to obtain a mean Reynolds number for a characteristic length L_H, which was already used in the Froude number calculation. After obtaining the

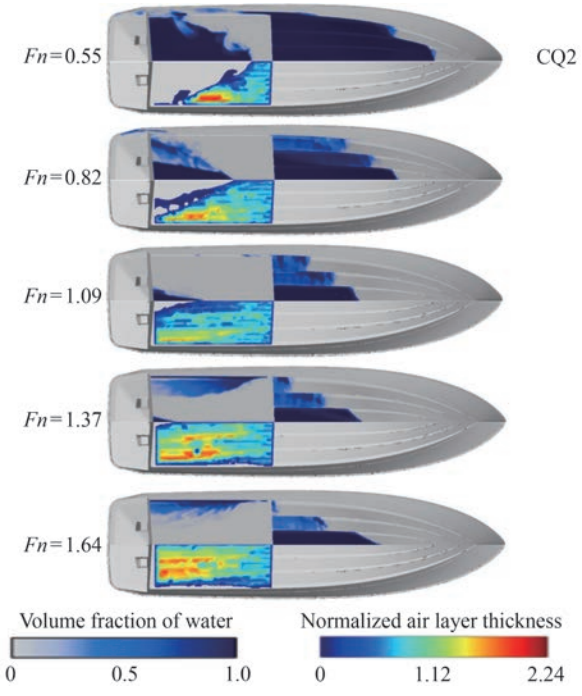

Figure 13 Air layer thickness and volume fraction of water contour plot for CQ2

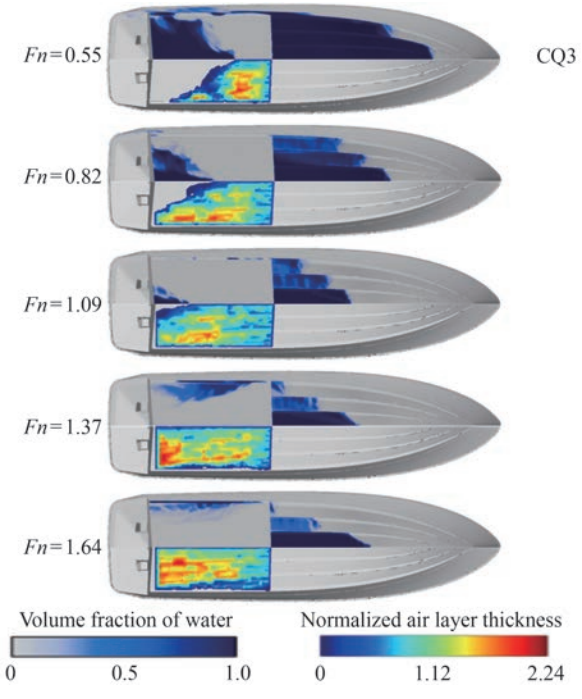

Figure 14 Air layer thickness and volume fraction of water contour plot for CQ3

Reynolds number corresponding to the mean of the tested hull velocities, δ has been calculated considering a turbulent flow (Schlichting and Gersten, 2016).

$$\delta = 0.37 \cdot L_H \cdot Re^{-1/5} = 0.11 \text{ m} \quad (3)$$

For each CQ condition, the colour bar scale remains fixed. As CQ increases and the hull velocity remains constant, the air trapped beneath the hull fills the air control volume (defined in Figure 5) more extensively, so both the Mean and Maximum air thickness increase as a result. The numerical values of both the Normalized Mean and Maximum Air Layer Thickness calculated for every condition by the Metro tool in MeshLab are reported in Table 7 and Table 8. The values are plotted in Figure 15 and Figure 16.

Table 7 Maximum air layer thickness for every motion condition

Fn	Normalized maximum air layer thickness		
	CQ1	CQ2	CQ3
0.55	1.77	1.96	2.03
0.82	1.68	1.84	1.94
1.09	1.47	1.57	1.82
1.37	1.75	2.03	2.16
1.64	1.65	1.87	2.03

Table 8 Mean air layer thickness for every motion condition

Fn	Normalized mean air layer thickness		
	CQ1	CQ2	CQ3
0.55	0.37	0.41	0.47
0.82	0.41	0.47	0.56
1.09	0.44	0.47	0.58
1.37	0.40	0.47	0.53
1.64	0.38	0.50	0.52

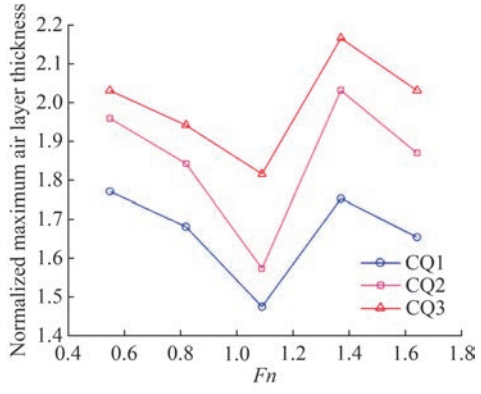

Figure 15 Maximum air layer thickness plot

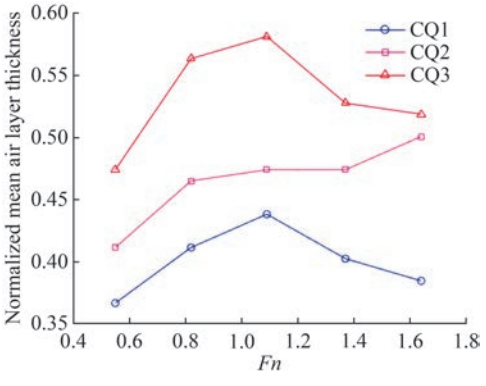

Figure 16 Mean air layer thickness plot

From Figure 15, it is evident that the maximum thickness of the air layer decreases with a decrease in CQ. Additionally, for the same CQ, the maximum thickness value shows different trends under different hull speed conditions. The maximum air layer thickness decreases going towards higher hull speeds in non-planing conditions, and it increases between *Fn* = 1.09 and 1.37. As the hull speed continues to increase beyond *Fn* = 1.37, the maximum air layer thickness starts decreasing again.

From the plot of mean air layer thickness in Figure 16, in non-planing conditions, the Mean air layer thickness increases for every CQ.

As the hull velocity increases above *Fn* = 1.09, the airflow tends to distribute more evenly across the step, resulting in a reduction in the average thickness. This effect has been observed as expected for both CQ1 and CQ3. However, it appears to deviate from the expected behaviour for CQ2, where the cushion tends to increase in thickness: this is because, at that flow rate, complete step filling occurs at a higher velocity (see Figure 13).

In Figure 17, normalized resistance variation for CQ1, CQ2 and CQ3 calculated as $\frac{R - R(\mathrm{CQ0})}{R}$ was plotted as a function of normalized ventilated area and of normalized mean air layer thickness.

Figure 17(a) confirms that going towards higher *Fn*, as expected, leads to an increase of $S_{v,n}$. In the planing region, a higher $S_{v,n}$ corresponds to a lower hull resistance, but the trend reverses in the semi-planing and displacement regions. A parabolic trend of the resistance can be discerned: the normalized resistance variation values are between 0 and −0.05 at *Fn* = 0.55, then they reach higher values at *Fn* = 0.82 and then they decrease until *Fn* = 1.64.

Figure 17(b) shows that a higher mean air layer thickness leads to a greater resistance reduction only for *Fn* = 0.55, *Fn* = 1.37 and *Fn* = 1.64. In the semi-planing region, a higher mean air layer thickness does not correspond to a resistance reduction.

Analysing the plots of Mean and Maximum thickness it becomes apparent that the distribution of the air layer changes with hull speed and CQ values. To account for this, the air direction ratio (ADR) was introduced and it was defined as the ratio between the air flowing through the side of the hull and the air flowing through the transom surface (see Table 2 and Figure 5). The ADR parameter is essential to capture how the air layer spatial distribution changes with different speeds and CQ values, providing valuable insights into the overall air trapping characteristics beneath the hull.

When the value is less than 1, it means that the air layer is developed towards the chine; when the value is greater than 1, the air layer is developed towards the transom, so the air escapes from behind the hull without branching out towards the chine on the left and on the right. Figure 18 shows an instance of the behaviour of the airflow for

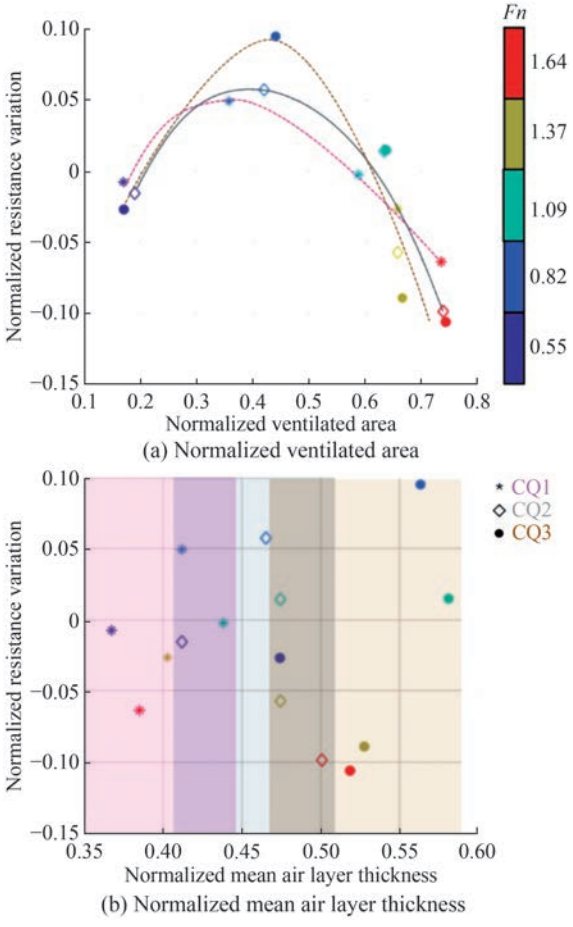

Figure 17 Scatter plots for normalized resistance variation

ADR < 1 and ADR > 1. The ADR < 1 instance is from the simulation with *Fn* = 0.82 and CQ = 1: in this case the airflow introduced from the step deviates towards the chine and escapes laterally. The ADR > 1 instance is from the simulation with *Fn* = 1.64 and CQ = 3: the airflow is now directed towards the transom, with almost no lateral escape.

The trend of ADR for every velocity is reported in Figure 19. ADR is less than 1 only at *Fn* = 0.55 and 0.82

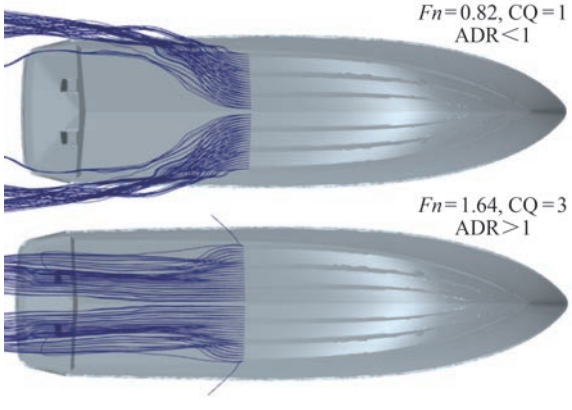

Figure 18 Different behaviour of the airflow for ADR < 1 and ADR > 1 (bottom view)

for CQ1, CQ2 and CQ3; only for CQ1, ADR is less than 1 even at *Fn* = 1.09. This means that the air layer is branching out in two sides, going towards the left and right chines. At *Fn* = 1.09, ADR is greater than 1 for both CQ2 and CQ3; after this point, for every air velocity, ADR is greater than 1, increasing in its value from *Fn* = 1.09 to *Fn* = 1.37 and decreasing from *Fn* = 1.37 to *Fn* = 1.64.

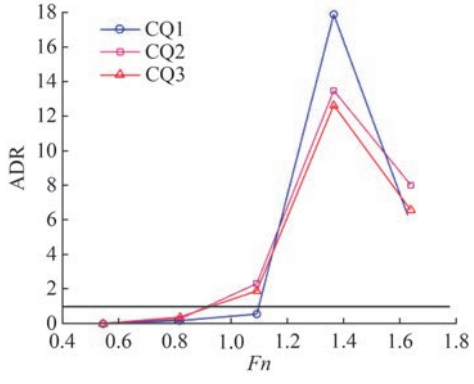

Figure 19 Air dissipation ratio plot

Another parameter defined is the spray rails airflow fraction (SRAF), which has been plotted in Figure 20. This value has been defined to check how much of the airflow under the hull is transported by the spray rails and how much is introduced from the air injection. For every CQ, the trend of the SRAF is always increasing with the velocity of the hull, arriving to a maximum value at *Fn* = 1.64. The trends for different CQs are practically overlapped until a velocity of 1.37; only at *Fn* = 1.64 the trends diverge clearly, with the SRAF being approximately 26% for CQ1, 17% for CQ2 and around 15% for CQ3. This means that the 26% of the air trapped under the hull comes from the spray rails for CQ1, but this effect becomes less important as the velocity of the injected air increments.

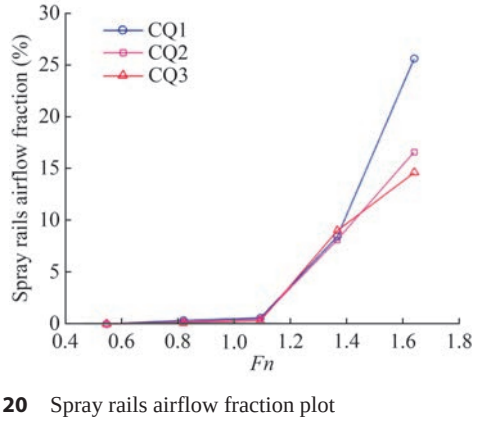

Figure 20 Spray rails airflow fraction plot

Another data visualization method has been introduced using three of the main parameters that define the fluid dynamics behaviour of the stepped hull: the CQ, the hull velocity and the air volume trapped under the hull.

These values have been condensed in a 3D surface coloured by the hull resistance values (Figure 21). Two main zones can be highlighted: a low-hull resistance zone and a high-hull resistance zone.

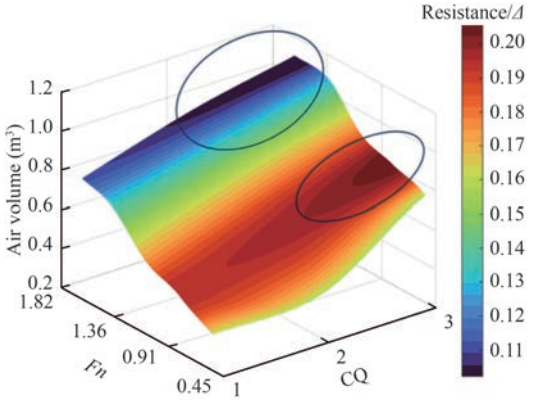

Figure 21 3D surface plot

Looking at the colourmap, the higher hull resistance is obtained for CQ3 at *Fn* = 1.09, and it remains high even for the lower CQs at the same hull velocity. The hull resistance decreases with the increase of the hull velocity, reaching a minimum at *Fn* = 1.64 between CQ2 and CQ3. At *Fn* = 1.64, the effort of going from CQ2 to CQ3 is not justified by a major hull resistance reduction.

4 Conclusions

In conclusion, this scientific study investigated the effects of air injection beneath the hull of a modified fast boat using a 2-DOF multiphase CFD simulation. The introduction of two new dimensionless parameters, referred to as ADR and SRAF, along with the utilization of novel graphical representation methods such as the air layer local thickness visualization, represent innovations in the critical analysis of the air injected thickness distribution of these hulls. The developed CQ map serves as a useful tool to establish the optimal air injection velocity for each hull velocity. By comparing the performance of the baseline hull with that of a stepped hull without air insufflation, it was established that the modifications did not result in performance degradation. Various scenarios were examined, varying both hull speed and air injection rate. The introduction of air injection yielded hull resistance reduction only in planing condition and it's therefore not recommended below *Fn* = 1.09 (Figure 10). At *Fn* = 1.09 the maximum achievable hull resistance reduction is the same for CQ0 and CQ1, so the effort of activating the ventilation is not justified. At *Fn* = 1.37 the optimal CQ is CQ3, with the hull resistance going down to the 83.6% of the baseline value. The most notable hull resistance reduction was achieved at *Fn* = 1.64. The hull resistance reduction for CQ2 and CQ3 is similar

(76.8% of the baseline for CQ2 against 76.2% for CQ3). The increment of the air injection rate to CQ3 shows limited improvements, so the recommended CQ to adopt at Fn = 1.64 is CQ2. Furthermore, a geometric analysis of the air layer beneath the hull was conducted, assessing its shape, extent, and characteristics as the hull velocity and air injection rate varied. Analysing the ADR, it was observed that higher hull and air speeds lead to a greater tendency for the air layer to develop centrally towards the transom, as opposed to branching into two separate layers. Additionally, the hull geometry was found to influence the airflow, drawing air from the spray rails as proven by the SRAF value. The contribution of this additional air on the total airflow under the hull becomes less significant as CQ increases. The CQ map can be used to adapt the air injection velocity through different operating conditions and to avoid performance or efficiency loss during navigation. The CFD method proposed in the paper has been validated and an uncertainty analysis has been conducted. It represents a good alternative in design phase to experimental setups which are expansive for this kind of hulls (power system for insufflation of air, hull with a step, bottom of the hull manufactured in Plexiglas for visualizing the air distribution). Considering these findings, the study highlights the substantial benefits of air insufflation in reducing hull resistance for high-speed hulls operating in planing conditions. Many other studies must be conducted in order to understand for example the impact of the sea-state on the efficiency of the system, another important aspect is the assessment of the power used for the injection of the air. Another aspect to investigate is the possible combination of the effects of the natural ventilation by the sides of a step and the effects of the artificial ventilation by means of air injection.

As a potential direction for future work, the incorporation of experimental validation techniques, such as particle image velocimetry (PIV), could provide valuable benchmarks to further assess the CFD-predicted air distribution. Although the numerical methods employed in this study offer significant advantages in terms of flexibility and resolution, experimental data could complement these simulations by offering direct measurements of air layer thickness and flow characteristics. Combining both approaches would lead to a more comprehensive understanding of the impact of air injection on resistance and wave dynamics.

The current study provides a strong foundation for future research and new promising topics, as the exploration of air insufflation remains a subject of contemporary interest within naval architecture and hydrodynamics.

Appendix A: Validation of the simulation

The first paper proposed by the authors for the validation of the CFD simulation is Cucinotta et al. (2018a). Table 3 of that paper shows the numerical setup used during the simulations validated with experimental setup. The solver is an implicit unsteady solver, the method used for coupling the continuity and momentum equation is the SIMPLE algorithm and the approach is segregated. The convention terms have been modelled with a 2nd order method and the turbulence model used is a Menter $k-\omega$. The temporal discretization was 2nd order and the time step was defined with the value suggested by ITTC. The gradients were modelled with an hybrid method (Gauss-LSQ). The algebraic system was solved with the Multigrid method. The interaction between water and air was modelled with the Volume of Fluid with an HRIC scheme for capturing the interface (high resolution interface capturing). The method for solving the motion of the ship is dynamic fluid body interaction with 10 inner steps. The motion of the hull was managed with the Overset method. Also, Cucinotta et al. (2019) and Cucinotta et al. (2021a) report the same CFD methods but on different geometric hulls. The authors for this paper have used that methodology with small differences dictated by new features implemented inside the simulation software. The boundary conditions with respect to validated method are the same, the algorithm used for coupling the continuity and momentum equation is the same and the approach also in this case is segregated. The convention terms are modelled with a 2nd order approach and the VOF scheme with the relative equation for capturing the interface is the same. There are differences in terms of turbulence model used, in terms of type of enclosure for overset region and in the scheme of discretization of the temporal term. To validate the method used in this paper, the authors conducted a set of simulations (three different velocities at a fixed airflow rate) on a hull, with its experimental data reported in Cucinotta et al. (2018a). As shown in Table A1, the modifications made to the numerical setup did not impact the quality of the final results, which consistently remained well within a 10% deviation.

Table A1 Validation results for monostep hull from Cucinotta et al. (2018a) and for an airflow rate of 6 500 L/min

Fn	Hull resistance/Δ		Resistance difference (CFD vs EXP) (%)	τ		τ difference (CFD vs EXP) (%)
	EXP	CFD		EXP	CFD	
0.77	0.136	0.141	3.608	3.990	4.150	3.855
1.02	0.161	0.159	−1.463	5.330	5.690	6.327
1.36	0.166	0.158	−5.063	5.420	5.450	0.550

Appendix B: Uncertainty analysis

In order to investigate the value of uncertainty of the simulation, an analysis has been conducted following the guidelines proposed by ITTC (2017). There are different sources of uncertainty during a CFD simulation, the main ones are: sources due to iteration (U1), sources due to size of mesh (UG) and the source relative to time-step (UT). Usually, as reported by Stern et al. (2001), the magnitude of the source relative to the grid is an order greater than the other two and it is the quantity to be verified during a campaign of CFD simulations. The approach is to use the same setup of the CFD simulation on three different meshes (fine, medium and coarse), the three meshes must have a size-ratio constant (r_k). The value of the solution of the nth parameter is: S_{n1}, S_{n2} and S_{n3} (respectively parameter on fine mesh, medium mesh and coarse mesh). It is possible to calculate the difference between the solution parameters (rate change) on medium-fine and coarse-medium meshes.

$$\varepsilon_{n,21} = S_{n2} - S_{n1} \tag{B1}$$

$$\varepsilon_{n,32} = S_{n3} - S_{n2} \tag{B2}$$

The two rate changes are used to calculate the convergence ratio R_G and the order of accuracy of the simulation.

$$R_G = \frac{\varepsilon_{n,21}}{\varepsilon_{n,32}} \tag{B3}$$

$$P_G = \frac{\ln\left(\frac{\varepsilon_{n,21}}{\varepsilon_{n,32}}\right)}{\ln r_K} \tag{B4}$$

The value of the convergence ratio is important for understanding if the sensitivity analysis has a monotonic convergence, oscillatory convergence, oscillatory divergence or monotonic divergence as defined in Table B1.

Table B1 Convergence analysis

Value of convergence ratio	Evaluation of convergence
$0 < RG < 1$	Monotonic convergence
$RG < 0 \,\&\, \lvert RG \rvert < 1$	Oscillatory convergence
$RG > 0$	Monotonic divergence
$RG < 0 \,\&\, \lvert RG \rvert > 1$	Oscillatory divergence

Thanks to the generalized method proposed by Richardson and suggested by the guidelines, the value of uncertainty can be calculated with the equation:

$$U_n = F_S \left| \frac{\varepsilon_{n,21}}{R_G^{P_G} - 1} \right| \tag{B5}$$

The uncertainty analysis has been carried out for the Fn = 1.64 and CQ3 condition. The value of size-mesh ratio is 1.59 and Table 11 shows the results of the uncertainty analysis. The most important result is the monotonic convergence of the mesh.

Table B2 Uncertainty analysis

Parameter	Elements	Resistance/Δ	τ (°)	W_{area} (m^2)
Fine	2025924	1.010	3.730	2.250
Medium	1273841	1.020	3.700	2.300
Coarse	801157	1.070	3.650	2.400
ε_{n21}	–	0.020	−0.030	0.050
ε_{n32}	–	0.050	−0.050	0.100
R_G	–	0.300	0.600	0.500
P_G	–	2.580	1.100	1.490
$R_G^{P_G}$	–	0.040	0.570	0.350
U_n	–	0.015	0.070	0.078

Nomenclature

g	Gravity acceleration (m/s^2)
V_H	Hull velocity (m/s)
V_A	Air velocity (m/s)
$Fn = \frac{V_s}{\sqrt{g \cdot L_H}}$	Froude number
L_{OA}	Overall length (m)
L_H	Hull length (m)
BPT	Beam at transom (m)
BPX	Maximum beam (m)
DPT	Depth (m)
DFT	Draft (m)
β	Deadrise angle (°)
Δ	Full load displacement (t)
L_{CG}	Longitudinal centre of gravity (m)
V_{CG}	Vertical centre of gravity (m)
N_{ST}	Number of steps
L_{ST}	Position of the step relative to the transom (m)
$B_{IN} \times H_{IN}$	Stepdimensions-half basis × height (m × m)
Q_T	Air mass flow rate through transom surface (kg/s)
Q_Y	Air mass flow rate through Y surface (kg/s)
Q_{PS}	Air mass flow rate through pre-step surface (kg/s)
$S_{w,n} = \frac{S_w}{S_w + S_v}$	Normalized wet area
$S_{v,n} = \frac{S_v}{S_w + S_v}$	Normalized ventilated area
$ADR = \frac{Q_T}{Q_Y}$	Air direction ratio

$$\mathrm{SRAF} = \frac{Q_{\mathrm{PS}}}{Q_T + Q_Y}$$ Spray rails airflow fraction

$$\mathrm{CQ} = \frac{V_A}{V_H}$$ Flow rate coefficient

Funding This work was partially supported by European Union funding (PON "Ricerca e Innovazione" 2014–2020).

Competing interest The authors have no competing interests to declare that are relevant to the content of this article.

References

Ahmadzadehtalatapeh M, Mousavi M (2016) A Review on the drag reduction methods of the ship hulls for improving the hydrodynamic performance. Int. J. Marit. Technol 4: 51-64

Amromin EL (2016) Analysis of interaction between ship bottom air cavity and boundary layer. Applied Ocean Research 59: 451-458. https://doi.org/10.1016/J.APOR.2016.03.009

Barberi E, Cucinotta F, Raffaele M, Salmeri F (2022) A hollowing topology optimization method for additive and traditional manufacturing technologies. Lecture Notes in Mechanical Engineering, Rome, 422-430. https://doi.org/10.1007/978-3-030-91234-5_43

Basin AM, Butuzov AA, Ivanov AN, Olenin Y, Petrov VI, Potapov OF, Ratner Y, Starobinskiy VB, Eller AO (1968) Ship motion when blowing air under its bottom. Sudostroyeniye (Soviet Shipbuilding) [USSR], 3-8

Busetto B, Bordignon A, Bortoluzzi A, Milanesi S, Paduano A, Mio A (2022) Life cycle assessment in the naval sector: between certification and new materials. Progress in Marine Science and Technology 6: 564-571. https://doi.org/10.3233/PMST220067

Butterworth J, Atlar M, Shi W (2015) Experimental analysis of an air cavity concept applied on a ship hull to improve the hull resistance. Ocean Engineering 110: 2-10. https://doi.org/10.1016/J.OCEANENG.2015.10.022

Butuzov AA, Vasin AI, Drozdov AL, Ivanov AN, Kalyuzhny VG, Matveev II, Ruzanov VE (1988) Full-scale trials of a boat with an air cavity. Shipbuild. Probl. 28: 45-51

Chen X, Yu L, Liu LY, Yang L, Xu S, Wu J (2023) Multi-objective shape optimization of autonomous underwater vehicle by coupling CFD simulation with genetic algorithm. Ocean Engineering 286: 115722. https://doi.org/10.1016/J.OCEANENG.2023.115722

Cignoni P, Callieri M, Corsini M, Dellepiane M, Ganovelli F, Ranzuglia G (2008) MeshLab: an open-source mesh processing tool. In: Scarano, V., De Chiara, R., Erra, U. (Eds.), Eurographics Italian Chapter Conference, the Eurographics Association, 129-136

Cignoni P, Rocchini C, Scopigno R (1998) Metro: measuring error on simplified surfaces. In: Computer Graphics Forum, Blackwell Publishers, 167-174

Cucinotta F, Guglielmino E, Sfravara F (2019) A critical CAE analysis of the bottom shape of a multi stepped air cavity planing hull. Applied Ocean Research 82: 130-142. https://doi.org/10.1016/J.APOR.2018.11.003

Cucinotta F, Guglielmino E, Sfravara F (2017a) An experimental comparison between different artificial air cavity designs for a planing hull. Ocean Engineering 140: 233-243. https://doi.org/10.1016/J.OCEANENG.2017.05.028

Cucinotta F, Guglielmino E, Sfravara F, Strasser C (2018a) Numerical and experimental investigation of a planing air cavity ship and its air layer evolution. Ocean Engineering 152: 130-144. https://doi.org/10.1016/J.OCEANENG.2018.01.071

Cucinotta F, Mancini D, Sfravara F, Tamburrino F (2021a) The effect of longitudinal rails on an air cavity stepped planing hull. J Mar Sci Eng 9(5): 470. https://doi.org/10.3390/JMSE9050470

Cucinotta F, Nigrelli V, Sfravara F (2018b) Numerical prediction of ventilated planing flat plates for the design of air cavity ships. International Journal on Interactive Design and Manufacturing (IJIDeM) 12: 537-548. https://doi.org/10.1007/s12008-017-0396-x

Cucinotta F, Nigrelli V, Sfravara F (2017b) A preliminary method for the numerical prediction of the behavior of air bubbles in the design of air cavity ships. Lecture Notes in Mechanical Engineering, Catania, 509-516. https://doi.org/10.1007/978-3-319-45781-9_51

Cucinotta F, Raffaele M, Salmeri F (2021b) A topology optimization method for stochastic lattice structures. Lecture Notes in Mechanical Engineering, 235-240. https://doi.org/10.1007/978-3-030-70566-4_38/FIGURES/3

Cucinotta F, Raffaele M, Salmeri F (2020) A topology optimization of a motorsport safety device. Lecture Notes in Mechanical Engineering, Modena, 400-409. https://doi.org/10.1007/978-3-030-31154-4_34

Cucinotta F, Raffaele M, Salmeri F, Sfravara F (2021c) A comparative life cycle assessment of two sister cruise ferries with diesel and liquefied natural gas machinery systems. Applied Ocean Research 112: 102705. https://doi.org/10.1016/J.APOR.2021.102705

Deng S, Suresh K (2017) Stress constrained thermo-elastic topology optimization with varying temperature fields via augmented topological sensitivity based level-set. Structural and Multidisciplinary Optimization 56: 1413-1427. https://doi.org/10.1007/S00158-017-1732-2

Di Bernardo R, Di Cecca B, Coppola T, Spazzafumo G, Speranza D (2024) Preliminary design of a 75 m Mega Yacht with diesel-Electric hybrid propulsion powered with hydrogen FCs. Int J Hydrogen Energy, in press. https://doi.org/10.1016/J.IJHYDENE.2024.06.412

Diez M, Lee EJ, Harrison EL, Powers AMR, Snyder LA, Jiang MJ, Bay RJ, Lewis RR, Kubina ER, Mucha P, Stern F (2022) Experimental and computational fluid-structure interaction analysis and optimization of deep-V planing-hull grillage panels subject to slamming loads—Part I: Regular waves. Marine Structures 85: 103256. https://doi.org/10.1016/J.MARSTRUC.2022.103256

Gao T, Wang Y, Pang Y, Cao J (2016) Hull shape optimization for autonomous underwater vehicles using CFD. Engineering Applications of Computational Fluid Mechanics 10: 599-607. https://doi.org/10.1080/19942060.2016.1224735

Ghadimi P, Sajedi SM, Sheikholeslami M, Ghadimi A (2023) Numerical study of the effect of angle and location of the first and second steps on the performance of planing hull and their optimization using the Taguchi statistical method. Math Probl Eng 2023: 1-18. https://doi.org/10.1155/2023/6881630

Gokcay S, Insel M, Odabasi AY (2004) Revisiting artificial air cavity concept for high speed craft. Ocean Engineering 31: 253-267. https://doi.org/10.1016/J.OCEANENG.2003.05.002

Hou S, Zhang Z, Lian H, Xing X, Gong H, Xu X (2022) hull shape optimization of small underwater vehicle based on Kriging-based response surface method and multi-objective optimization algorithm. Brodogradnja: An International Journal of Naval Architecture and Ocean Engineering for Research and Development 73: 111-134. https://doi.org/10.21278/BROD73307

ITTC (2017) Uncertainty analysis in CFD verification and validation

methodology and procedures. ITTC–Recommended Procedures and Guidelines, 1-13

Latorre R (1997) Ship hull drag reduction using bottom air injection. Ocean Engineering 24: 161-175. https://doi.org/10.1016/0029-8018(96)00005-4

Matveev KI (2003) On the limiting parameters of artificial cavitation. Ocean Engineering 30: 1179-1190. https://doi.org/10.1016/S0029-8018(02)00103-8

Matveev KI (2015) Hydrodynamic modeling of semi-planing hulls with air cavities. International Journal of Naval Architecture and Ocean Engineering 7: 500-508. https://doi.org/10.1515/IJNAOE-2015-0036

Matveev KI (2020) Simplified model for unsteady air cavities under ship hulls. Proceedings of the Institution of Mechanical Engineers Part M: Journal of Engineering for the Maritime Environment 234: 100-107. https://doi.org/10.1177/1475090219862898/ASSET/IMAGES/LARGE/10.1177_1475090219862898-FIG9.JPEG

Mio A, Fermeglia M, Favi C (2022) A critical review and normalization of the life cycle assessment outcomes in the naval sector. Articles description. J Clean Prod 370: 133476. https://doi.org/10.1016/J.JCLEPRO.2022.133476

Nazemian A, Ghadimi P (2022a) Shape optimisation of trimaran ship hull using CFD-based simulation and adjoint solver. Ships and Offshore Structures 17: 359-373. https://doi.org/10.1080/17445302.2020.1827807

Nazemian A, Ghadimi P (2022b) Multi-objective optimization of ship hull modification based on resistance and wake field improvement: combination of adjoint solver and CAD-CFD-based approach. Journal of the Brazilian Society of Mechanical Sciences and Engineering 44: 1-27. https://doi.org/10.1007/S40430-021-03335-4/METRICS

Nazemian A, Ghadimi P (2021a) CFD-based optimization of a displacement trimaran hull for improving its calm water and wavy condition resistance. Applied Ocean Research 113: 102729. https://doi.org/10.1016/J.APOR.2021.102729

Nazemian A, Ghadimi P (2021b) Automated CFD-based optimization of inverted bow shape of a trimaran ship: an applicable and efficient optimization platform. Scientia Iranica 28: 2751-2768. https://doi.org/10.24200/SCI.2020.56644.4833

Nimmagadda NVR, Polisetty LR, Vaidyanatha Iyer AS (2020) Simulation of air–water interface effects for high-speed planing hull. Journal of Marine Science and Application 19: 398-414. https://doi.org/10.1007/S11804-020-00172-0/FIGURES/26

Pearce BW, Brandner PA, Foster SJ (2015) Ventilated cavity flow over a backward-facing step. J Phys Conf Ser 656: 012164. https://doi.org/10.1088/1742-6596/656/1/012164

Plocher J, Panesar A (2019) Review on design and structural optimisation in additive manufacturing: Towards next-generation lightweight structures. Mater Des 183: 108164. https://doi.org/10.1016/J.MATDES.2019.108164

Schlichting H, Gersten K (2016) Boundary-layer theory. Springer Berlin, Heidelberg, 1-799. https://doi.org/10.1007/978-3-662-52919-5/COVER

Stern F, Wilson RV, Coleman HW, Paterson EG (2001) Comprehensive approach to verification and validation of CFD simulations—Part 1: Methodology and procedures. J Fluids Eng 123: 793-802. https://doi.org/10.1115/1.1412235

Sulman M, Mancini S, Bilandi RN (2024) Numerical investigation of single and double steps in planing hulls. J Mar Sci Eng 12(4): 614. https://doi.org/10.3390/JMSE12040614

Tavakoli S, Zhang M, Kondratenko AA, Hirdaris S (2024) A review on the hydrodynamics of planing hulls. Ocean Engineering 303: 117046. https://doi.org/10.1016/j.oceaneng.2024.117046

Wheeler MP, Ryan P, Cimolin F (2021) Using VOF slip velocity to improve productivity of planing hull CFD simulations. SNAME International Conference on Fast Sea Transportation 2021, FAST 2021, SNAME-FAST-2021-013. https://doi.org/10.5957/FAST-2021-013

Yan J, Xu Q, Zhang Q, Fan ZR, Du HZ, Geng DL, Yan K, Niu B (2021) Current and future trends of artificial intelligence in the field of structural topology optimization. Chinese Journal of Computational Mechanics 2021(4): 412-422

Yan X, Zhu J, Kuang M, Wang X (2019) Aerodynamic shape optimization using a novel optimizer based on machine learning techniques. Aerosp Sci Technol 86: 826-835. https://doi.org/10.1016/J.AST.2019.02.003